The Thesis Committee for Robert Anthony O'Donovan-Zavada
Certifies that this is the approved version of the following thesis:

Hierarchical Three-Dimensional Fe-Ni Hydroxide Nanosheet Arrays on Carbon Fiber Electrodes for Oxygen Evolution Reaction

APPROVED BY
SUPERVISING COMMITTEE:

Supervisor:

Arumugam Manthiram

Llewellyn Rabenberg

Hierarchical Three-Dimensional Fe-Ni Hydroxide Nanosheet Arrays on Carbon Fiber Electrodes for Oxygen Evolution Reaction

by

Robert Anthony O'Donovan-Zavada, B.A.

Thesis

Presented to the Faculty of the Graduate School of

The University of Texas at Austin

in Partial Fulfillment

of the Requirements

for the Degree of

Master of Science in Engineering

The University of Texas at Austin

May 2014

Acknowledgements

I am grateful to my family, especially my mother, father, and sister, for the support they have given me over the years. I thank my advisor, Dr. Arumugam Manthiram, for his guidance during the course of this research work. I also appreciate Dr. Steve Feller at Coe College for his mentoring during my post-secondary education. I am thankful to Dr. Llewellyn Rabenberg for volunteering to serve on my thesis committee.

This research would not have been possible without the support of several colleagues. Dr. Longjun Li helped me from my very first day of graduate school, teaching me how to use several pieces of equipment and always being available to answer questions. Dr. Maiyalagan Thandavarayan's assistance was invaluable for this project; he provided much of the background knowledge that helped me develop different concepts and approaches. I would like to acknowledge funding from the U.S. Department of Energy, Office of Basic Energy Sciences, Division of Materials Sciences and Engineering, under award number DE-SC0005397.

I would like to thank Zach Moorhead, Eric Allcorn, and Philip Noell for their contributions to our weekly meetings where we discussed our research in a stress-free environment.

Abstract

Hierarchical Three-Dimensional Fe-Ni Hydroxide Nanosheet Arrays on Carbon Fiber Electrodes for Oxygen Evolution Reaction

Robert Anthony O'Donovan-Zavada, MSE

The University of Texas at Austin, 2014

Supervisor: Arumugam Manthiram

As demands for alternative sources of energy increase over the coming decades, water electrolysis will play a larger role in meeting our needs. The oxygen evolution reaction (OER) component of water electrolysis suffers from slow kinetics. An efficient, inexpensive, alternative electrocatalyst is needed. We present here high-activity, low onset potential, stable catalyst materials for OER based on a hierarchical network architecture consisting of Fe and Ni coated on carbon fiber paper (CFP). Several compositions of Fe-Ni electrodes were grown on CFP using a hydrothermal method, which produced an interconnected nanosheet network morphology. The materials were characterized by scanning electron microscopy (SEM) and X-ray diffraction (XRD). Electrochemical performance of the catalyst was examined by cyclic voltammetry (CV) and linear sweep voltammetry (LSV). The best electrodes showed favorable activity (23 mA/cm^2, 60 mA/mg), onset potential (1.42 V *vs*. RHE), and cyclability.

Table of Contents

List of Tables

List of Figures

Chapter 1: Introduction

The United States Energy Information Administration (EIA) recently released its International Energy Outlook (IEO) for 2013 [1]. The report predicts that the world's energy use will rise by 56% between 2010 and 2040, mostly in developing countries. It concludes that renewable energy will grow the fastest among all energy sources. Renewable energy is increasingly necessary due to current concerns regarding energy security, rising oil costs, and the impact fossil fuel emissions have on the environment. In the future, many countries are expected to enact policies that favor renewable energy over fossil fuels [1].

1.1 Water Splitting and Oxygen Evolution Reaction (OER)

Much work needs to be done in all areas of renewable energy in order to meet our future energy consumption demands. Efficient and economical conversion of electricity from sustainable energy sources (*e.g.*, solar, wind, and hydro) into hydrogen and oxygen by electrochemical water splitting is one of our greatest challenges [2-18].

Hydrogen is the lightest element in the periodic table and has the highest energy density by mass at 143 MJ/kg [19]. Myriad uses exist for hydrogen in industrial applications: as a reactant in the electronics and petroleum industries, as a coolant in

electrical generators, and as an oxygen scavenger to chemically remove O_2 to prevent corrosion [20]. Perhaps the most important future use for hydrogen will be for fuels.

Used directly, hydrogen is the cleanest burning fuel. It is more efficient than gasoline, which makes it viable for use in automobiles and aviation with the added benefit of reduced emissions. Hydrogen fuel is already being used in the aerospace industry. One of the biggest areas of concern associated with hydrogen use is the high cost of storage [21].

Hydrogen can also be used for fuel in fuel cells. This topic has received considerable attention in the scientific community in recent years [2, 22]. Many fuels are used in fuel cells, but hydrogen is the most common. The hydrogen fuel cell process consists of water splitting in reverse; it converts hydrogen and oxygen into electricity and water. All of these uses for hydrogen make water splitting a critical concept for further study.

Alkaline water splitting involves the following two half reactions: hydrogen evolution reaction (HER) at the cathode and oxygen evolution reaction (OER) at the anode, as given by equations (1) and (2), respectively. Combining these two half reactions yields equation (3) [7, 13, 15, 16].

HER $4H_2O + 4e^- \rightarrow 2H_2 + 4OH^-$ (1)

OER $4OH^- \rightarrow O_2 + 2H_2O + 4e^-$ (2)

$H_2O \rightarrow H_2 + 1/2O_2$ (3)

This research focuses on OER. OER is a complex four-electron oxidation process where each electron transfer corresponds to a proton transfer [13]. This process suffers from slow kinetics, leading to large overpotentials and, consequently, reduced efficiency [23]. In order to make OER easier with faster reaction kinetics, efficient and economical catalysts must be developed.

1.2 OER ELECTROCATALYSTS

Electrocatalysts, which function at the electrode surface, increase the rate of chemical reactions by lowering the activation energy [13]. Current commercial electrolyzers use ruthenium (Ru) and iridium (Ir) oxides as OER catalysts chosen for their high stability and catalytic activity [24]. However, the costs of Ru and Ir are prohibitive. Much effort has been expended in attempts to develop alternative, less expensive OER catalysts [25].

Recently, many catalysts for OER based on abundant 3d metals, such as iron (Fe), cobalt (Co), nickel (Ni), and manganese (Mn), have been developed with a focus on the efficiency and economics [5, 24, 26, 27]. Ni-containing materials such as binary Ni

oxides, Ni-containing mixed-metal oxides, and various Ni-containing perovskites, are low cost and abundant. They also exhibit moderate OER overpotentials under alkaline conditions [3, 4, 25, 28, 29]. $Ni(OH)_2$/NiOOH OER electrocatalysts have been used to study the role of metal impurities on the OER activity [30-33]. It was found that Fe and Ce impurities improved catalytic activity and Cd, Zn, and Pb caused catalytic activity to decrease.

The activity increase had a few possible causes. As Ni^{4+} is formed throughout the OER process, it is known to increase resistance [33]. The addition of Fe could increase the conductivity because less Ni^{4+} is formed. Fe-doping could also improve the activity because it provides more favorable sites for OER intermediates [30]. Knowing that some Fe-doping increases activity, we investigated the optimum amount of Fe needed to improve onset potential, catalytic activity, and cycling. First, we looked into the ideal structure and substrates to grow our material.

1.3 Layered Double Hydroxide (LDH) Electrocatalysts and Carbon Fiber Substrates

The structure of layered double hydroxides (LDHs) have been known for over 150 years [20]. They are comprised of a brucite-like structure, $Mg(OH)_2$, where the hydroxide ions surround the magnesium ions octahedrally. Through edge-sharing, these

octahedra create layers that can stack and form a three-dimensional structure [20], see Figure 1.

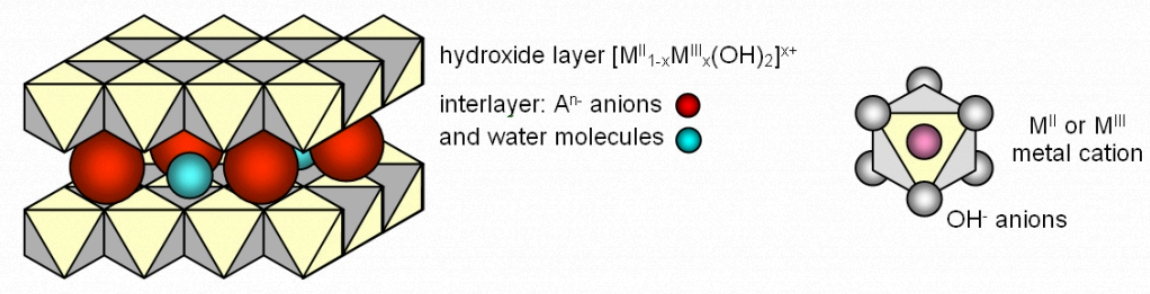

Figure 1: Structure of layered double hydroxides (LDHs). Image from [34].

The general formula for LDHs is $[M^{II}_{1-x}M^{III}_{x}(OH)_2][A^{n-}_{x/n}]\bullet mH_2O$ where M represents the metal ions and A the anions [35]. Recently, due to the unique structure of LDHs, research has focused on their many applications [36-42]. LDH applications have included use as absorbents [21, 25, 43, 44], anion exchangers [45, 46], biosensors [47, 48], and catalysts [5, 11, 27, 49-52].

Carbon fiber paper (CFP) is inexpensive, light, porous, and conductive. This means it is economically advantageous and multi-functional (*e.g.*, supercapacitors, secondary batteries, and water electrolyzers) [17, 18, 53-59]. Carbon fibers have been used as a substrate for growing materials [56, 60]. LDHs have been coated on CFP as electrodes for supercapacitors and secondary batteries, and have shown good performance [53, 54, 57].

Nickel hydroxide, $Ni(OH)_2$, is known to be highly stable, inexpensive, and catalytically active. This makes it a desirable alternative to the more expensive OER catalysts mentioned above [13, 16, 61]. The combination of LDHs, CFP, and Ni is beginning to show promising results as electrocatalysts for OER [17, 18]. Given this background, the objectives of this thesis are given below.

1.4 Thesis and Main Contributions

In this work, we investigate the combined role of iron and nickel as an electrocatalyst in alkaline media. We present a new method of loading Fe-Ni LDHs on CFP that exhibit excellent OER activity, stability, and onset potential in 0.1 M KOH electrolyte (pH = 13). These results show great promise in terms of design of catalysts for OER by using inexpensive and easily prepared Fe-Ni LDH materials.

Four samples of Fe-Ni LDHs on CFP were synthesized. They will be identified as, Fe-Ni 2:1, Fe-Ni 1:1, Fe-Ni 1:2, and Fe-Ni 1:10, where the ratios represent the relative amounts of $FeCl_2 \cdot 4H_2O$ and $Ni(NO_3)_2 \cdot 6H_2O$ used in the synthesis.

Chapter 2: Experimental Methods

2.1 Substrate Preparation

The CFP composite used in this work was purchased from Fuel Cell Earth. Specifically, Toray Paper 120 with 0% wet proofing (no Teflon treatment), dimensions of 40 cm x 40 cm and thickness of 370 μm was used. Before pretreatment, the CFP was cut into 2.3 cm x 8 cm strips to fit in a standard 40 mL autoclave. The CFP was pretreated with concentrated nitric acid (HNO_3) solution for 30 min. After nitric acid treatment, the CFP was cleansed four times using an ultrasonicator. The first cleaning was with deionized water, followed by acetone, a third with ethanol and finally finishing with deionized water. Each lasted for 10 min, after which the CFP was allowed to dry at room temperature [53].

2.2 Fe-Ni Nanosheet Synthesis

A typical synthesis procedure of Fe-Ni with nanosheet morphology is as follows: a combined total of 2 mmol of $FeCl_2 \cdot 4H_2O$ and $Ni(NO_3)_2 \cdot 6H_2O$ (Sigma-Aldrich) were dissolved in 40 mL of deionized water, as well as 30 mmol urea [35]. For Fe-Ni 2:1, 4/3 mmol of $FeCl_2 \cdot 4H_2O$ and 2/3 of $Ni(NO_3)_2 \cdot 6H_2O$ were mixed together. For Fe-Ni 1:1, 1 mmol each of $FeCl_2 \cdot 4H_2O$ and $Ni(NO_3)_2 \cdot 6H_2O$ were added. For Fe-Ni 1:2, 2/3 mmol of

$FeCl_2 \cdot 4H_2O$ and 4/3 of $Ni(NO_3)_2 \cdot 6H_2O$ were added. For Fe-Ni 1:10, 2/11 mmol of $FeCl_2 \cdot 4H_2O$ and 20/11 of $Ni(NO_3)_2 \cdot 6H_2O$ were added. The compositions are given in Table 1. The solution was then stirred for 10 min and transferred to a 40 mL Teflon-lined stainless steel autoclave. The treated CFP was put into the solution at 90° C for 6 h with a ramp rate of 3°/min up and 5°/min down. Afterwards, the sample was thoroughly washed with deionized water and dried at room temperature for 24 h [35].

Table 1: Sample compositions.

Fe:Ni	$FeCl_2 \cdot 4H_2O$		$Ni(NO_3)_2 \cdot 6H_2O$	
	(mmol)	(grams)	(mmol)	(grams)
2:1	4/3	0.1940	2/3	0.3880
1:1	1	0.1988	1	0.2910
1:2	2/3	0.1325	4/3	0.2651
1:10	2/11	0.0362	20/11	0.5290

This synthesis technique resulted in a uniform coating of material on the CFP, see Figure 2 (see Figures 4 and 5 for a microscopic view). The mass loading was approximately 0.4 mg/cm^2 for all samples.

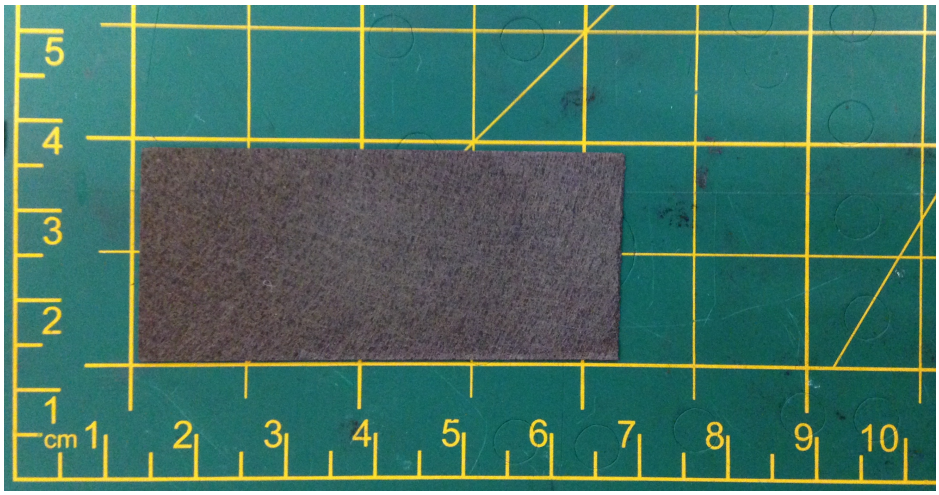

Figure 2: Uniform coating of Fe-Ni 2:1 on carbon fiber paper (CFP).

2.3 Analysis Techniques

X-ray diffraction (XRD) analysis was performed with a Phillips X-Ray Diffractometer using Cu K**α** radiation between 10° and 70°, with a step size of 0.2° and an integration time of 3 s. Scanning electron microscopy (SEM) images were collected with a JEOL-JSM-5610 microscope operated at 20 kV. Electrochemical tests were carried out with a three-electrode setup in a 0.1 M KOH aqueous solution made with deionized water (pH = 13), a Pt counter electrode, a saturated calomel electrode (SCE) as the reference electrode, and a 1 cm^2 electrode sample as the working electrode. Cyclic voltammograms (CVs) were recorded between 1.2 and 1.55 V *vs*. RHE at scan rates of 10, 20, 40, 80, 100, and 200 mV/s using a combined potentiostat/galvanostat (Autolab).

Linear sweep voltammetry (LSV) curves were gathered between 1.2 and 1.8 V *vs*. RHE at a scan rate of 20 mV/s. RHE values were calculated from experimental SCE values: $E_{RHE} = 0.241 - 0.0591*(pH)$ V = 0.241 – (-0.0591*(13)) V = E_{SCE} + 1.0093 V.

Chapter 3: Results and Discussion

3.1 X-RAY DIFFRACTION (XRD)

The XRD patterns of all four samples are shown in Figure 3. Peaks were observed at 11.54°, 23.65°, 26.56°, 34.51°, 43.12°, and 54.49°. The peaks at 26.56°, 43.12°, and 54.49° can be indexed to carbon from the CFP. The peak at 23.65° is only observable in Fe-Ni 1:1 and Fe-Ni 1:2 due to interference by the larger peak 26.56°. Peaks at 11.54°, 23.65°, and 34.51° were indexed to hexagonal $Fe_2Ni_2(CO_3)(OH)_8 \bullet nH_2O$. The prefered orientations of the samples are (003), (006), and (0012). Although $Fe_2Ni_2(CO_3)(OH)_8 \bullet nH_2O$ is most abundant, α-$Ni(OH)_2$ may exist in the samples. α-$Ni(OH)_2$ shows peaks at 11°, 23°, 34°, 39° and 60° (JCPDS No 38-0715). While no observable peak at 60° exists in our samples, the existence of α-$Ni(OH)_2$ in small amounts cannot be ruled out, and it may explain some electrochemical results discussed later in section 3.3.3.

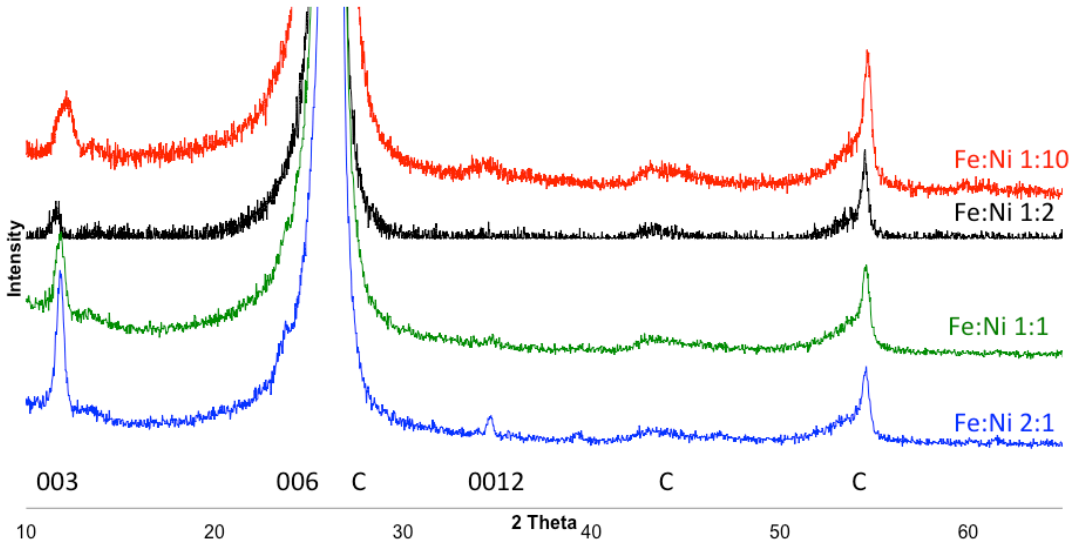

Figure 3: X-ray diffraction (XRD) of all four Fe-Ni samples synthesized.

3.2 Scanning Electron Microscopy (SEM)

Figures 4 and 5 show detailed morphology of the Fe-Ni LDH material uniformly coated on CFP. A closer look at this morphology reveals thin, smooth nanosheets of approximately 2 μm in length, estimated to be 10 nm thick. This morphology increases the surface area, thus increasing the catalytic activity. Conductivity is also aided because of the interconnectedness of the sheets; it allows multiple paths for ions to travel throughout the sample. The Fe-Ni 1:10 sample has slightly different morphology and excess material. The different morphology is likely due to the composition of the sample,

which is Ni-rich. The other compositions have a more even balance of Fe and Ni, which may facilitate the uniform nanosheet morphology.

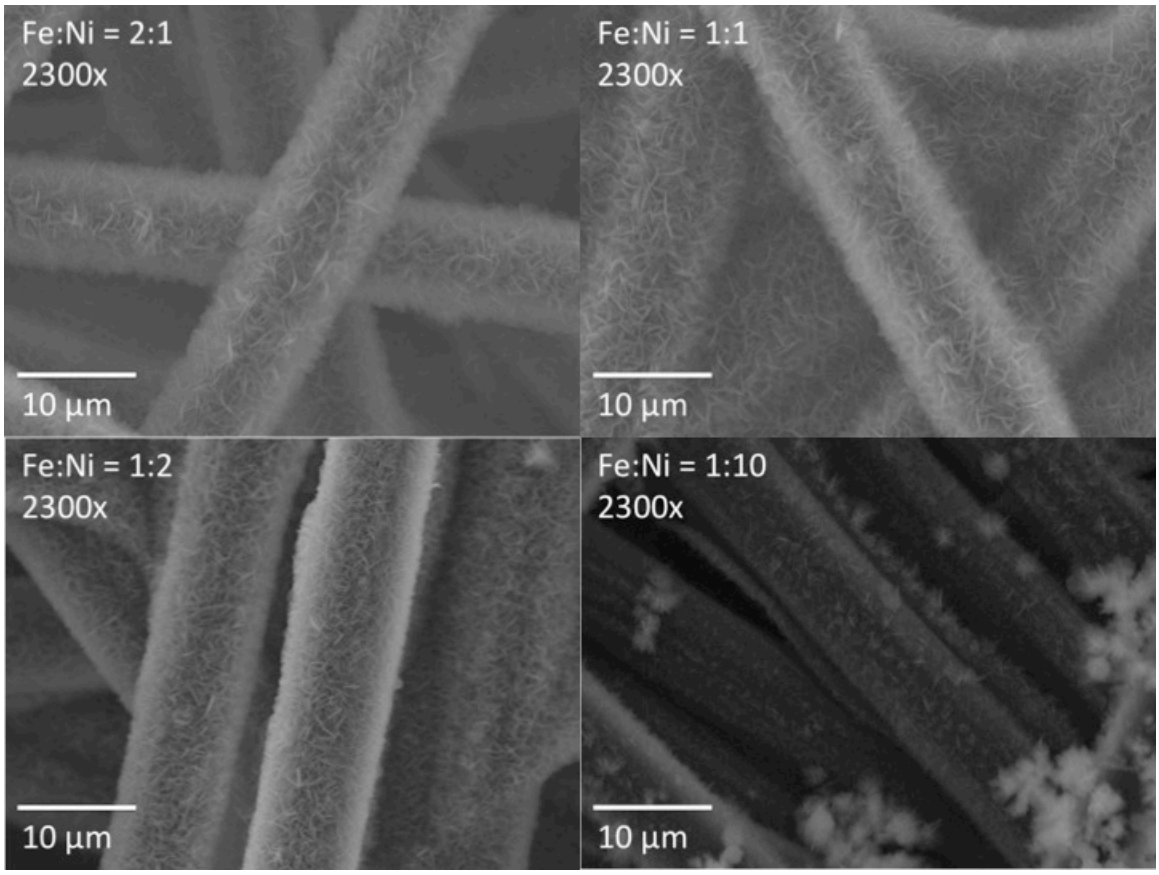

Figure 4: Scanning electron microscopy (SEM) images at a lower magnification of Fe-Ni 2:1, Fe-Ni 1:1, Fe-Ni 1:2, and Fe-Ni 1:10, showing uniform coating and morphology. The exception is Fe-Ni 1:10, which has excess material.

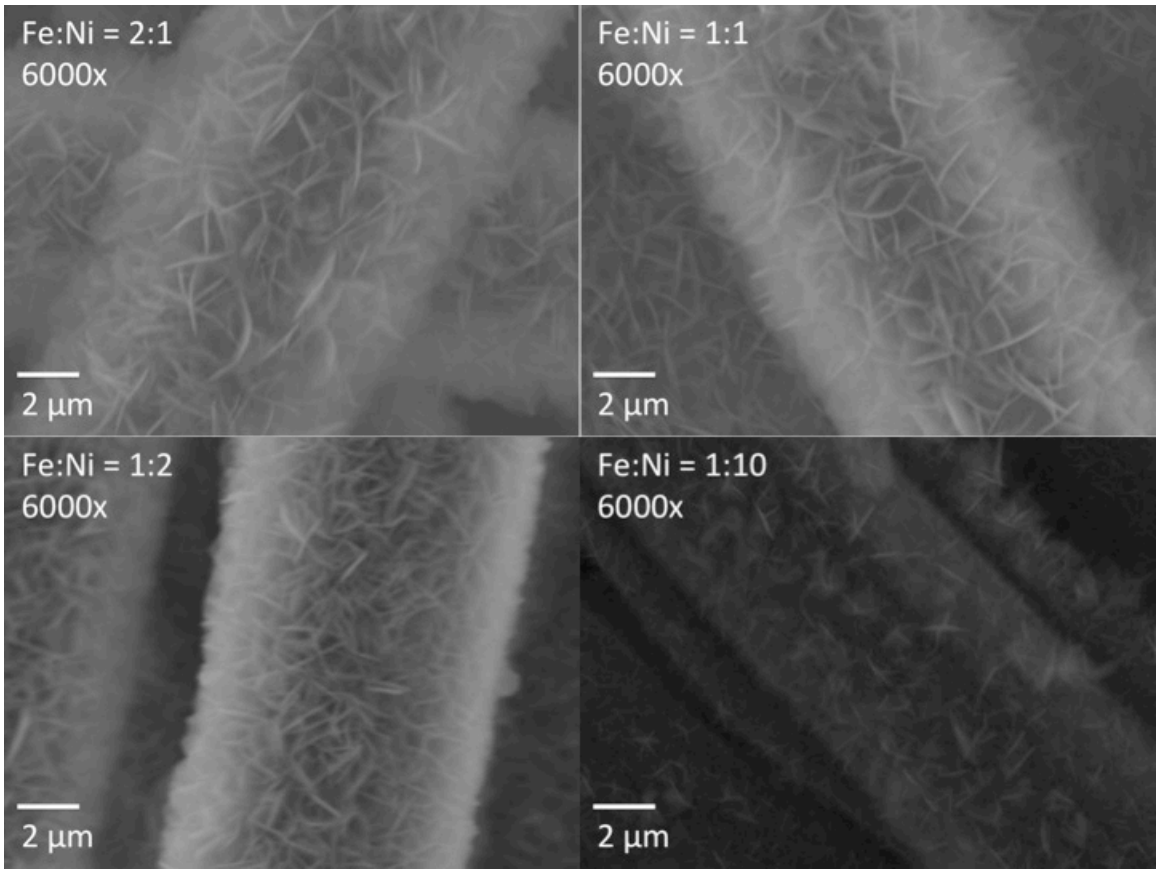

Figure 5: Scanning electron microscopy (SEM) images at a higher magnification of Fe-Ni 2:1, Fe-Ni 1:1, Fe-Ni 1:2, and Fe-Ni 1:10, showing uniform coating and morphology with the exception of Fe-Ni 1:10.

3.3 OXYGEN EVOLUTION REACTION (OER)

3.3.1 Cyclic Voltammetry (CV)

The cyclic voltammograms (CVs) for the first cycles of all four samples are shown in Figure 6 and Table 2, normalized to the electrode's geometric area and taken at sweep rates from 10 - 200 mV/s. For all samples, no anodic peaks were apparent prior to the onset of the OER during the forward sweep. During the reverse sweep, some of the samples exhibit a cathodic peak that is likely related to the reduction of Ni^{3+} (electrochemically generated during the forward sweep) to Ni^{2+}. At a 10 mV/s scan rate, Fe-Ni 2:1 shows no peak cathodic current (i_{pc}), and at a 100 mV/s scan rate, a very small i_{pc} of -0.03 mA exists at the peak cathodic potential (E_{pc}) of 1.42 V *vs*. RHE. Fe-Ni 1:1 shows a small i_{pc} of -0.04 mA at 1.46 V *vs*. RHE at 10 mV/s, and a larger i_{pc} of -0.46 mA at 1.46 V *vs*. RHE at 200 mV/s. Fe-Ni 1:2 has an i_{pc} of -2.68 mA at 1.37 V *vs*. RHE at 10 mV/s, and -5.07 mA at 1.34 V *vs*. RHE at 200 mV/s. Fe-Ni 1:10 shows an i_{pc} of -1.91 mA at 1.37 V *vs*. RHE at 10 mV/s, and an i_{pc} of -4.49 mA at 1.33 V *vs*. RHE at 200 mV/s. The magnitude of the cathodic peak is likely related to the amount of Ni in the sample. Fe-Ni 2:1 and 1:1 show no shift of E_{pc} with changing scan rates, while Fe-Ni 1:2 and Fe-Ni1:10 show a negative shift of E_{pc} with increasing scan rates. This trend may be indicative of the relative electronic conductivities of the electrodes: more Fe leads to higher conductivity, which in turn decreases the effects of electrode polarization with increased sweep rates and thus decreases the cathodic peak shift.

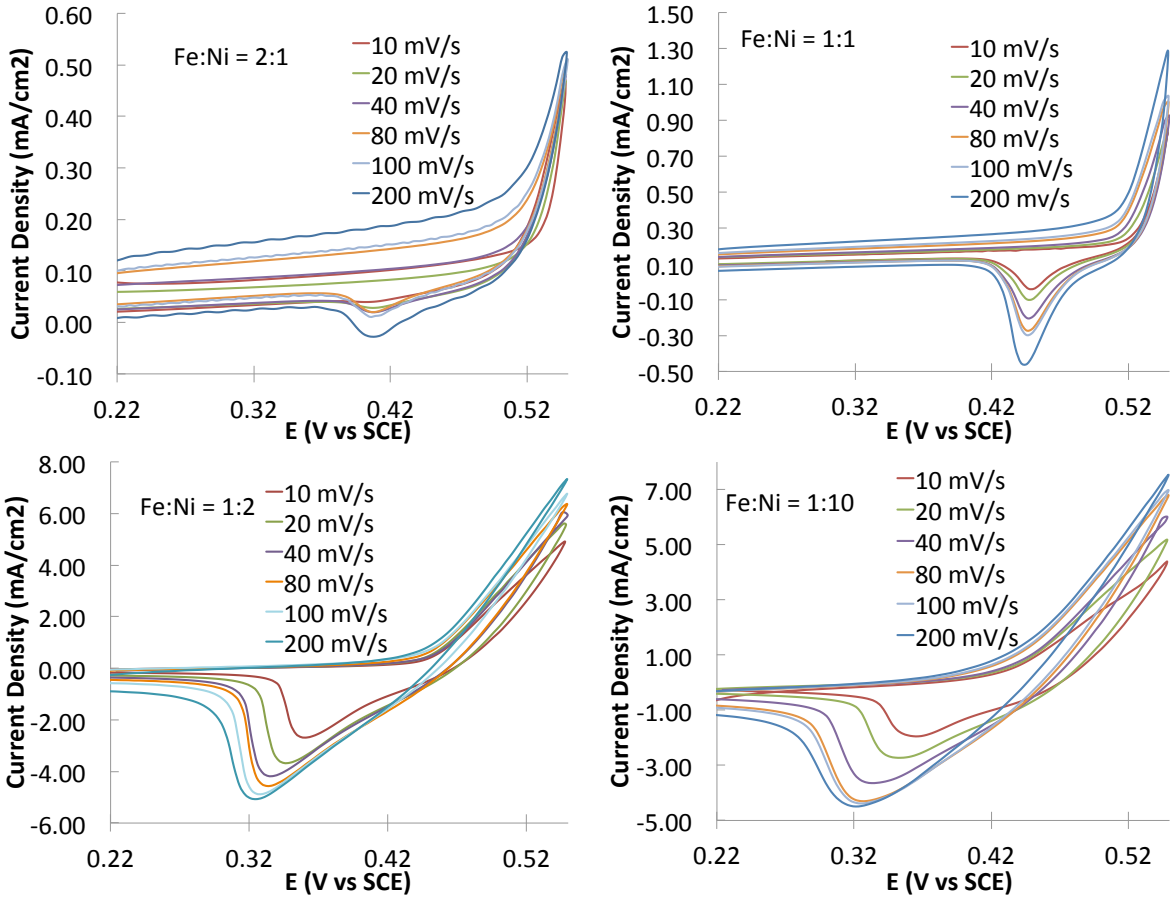

Figure 6: Cyclic Voltammetry (CV) profiles of Fe-Ni 2:1, Fe-Ni 1:1, Fe-Ni 1:2, and Fe-Ni 1:10, respectively.

Table 2: Variations of peak cathodic current and voltage with composition at different scan rates.

	10 mV/s		200 mV/s	
Fe:Ni	i_{pc} (mA)	E_{pc} (vs RHE)	i_{pc} (mA)	E_{pc} (vs RHE)
2:1	x	x	-0.03	1.42
1:1	-0.04	1.46	-0.46	1.46
1:2	-2.68	1.37	-5.07	1.34
1:10	-1.91	1.37	-4.49	1.33

3.3.2 Linear Sweep Voltammetry (LSV)

Several trends are evident when we examine LSV curves for our samples (Figure 7) taken at 20 mV/s and normalized to the electrode's geometric area. First, the Fe-Ni 1:2 and Fe-Ni 1:10 have very similar curves, with Fe-Ni 1:10 exhibiting a slightly lower onset potential (1.42 V compared to 1.45 V *vs*. RHE) but a lower activity (22.4 mA/cm^2 compared to 23.4 mA/cm^2) at 1.8 *vs*. RHE. Second, Fe-Ni 1:1 and Fe-Ni 2:1 have similar onset potentials (1.54 V compared to 1.55 V *vs*. RHE) as well, but different slopes. The OER current of Fe-Ni 1:1 increases faster and, at 1.8 V *vs*. RHE, is close to the activity of Fe-Ni 1:2 and Fe-Ni 1:10.

The results indicate that when the ratio of Ni to Fe increases, the OER onset potential decreases. We also see that, up to Fe-Ni 1:2, as the Ni to Fe ratio increases, the

activity increases. At Fe-Ni 1:10, the activity slightly decreases. This slight reduction in activity could be due to the morphological differences.

Table 3 shows a summary of the onset potentials and activity for the samples. We can conclude that the best performing materials, based on onset potential and activity criteria, are Fe-Ni 1:2 and Fe-Ni 1:10. Since Fe-Ni 1:2 and Fe-Ni 1:10 performed the best electrochemically, we next tested their cyclability.

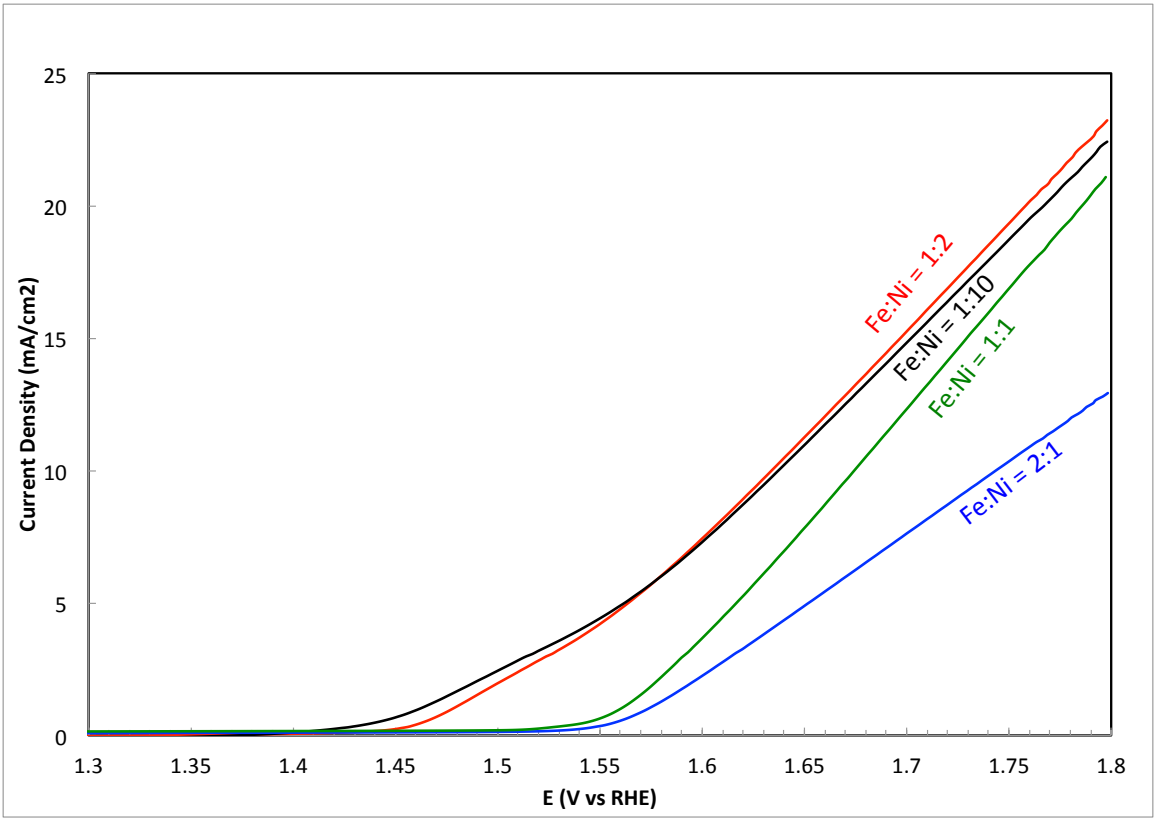

Figure 7: Linear sweep voltammetry (LSV), showing variations in onset potential and activity with composition, measured in 0.1 M KOH at a scan rate of 20 mV/s.

Table 3: Variations of onset potentials and activity with composition

Fe:Ni	Onset Potential V vs. RHE	Activity mA/cm² @ 1.8 V vs RHE	Mass Activity mA/mg @ 1.8 V vs RHE
2:1	1.55	12.8	32
1:1	1.54	21.1	52.75
1:2	1.45	23.4	58.5
1:10	1.42	22.4	56

3.3.3 LSV Cycle Tests

To test the electrochemical stability of the catalysts, we cycled the Fe-Ni 1:2 and Fe-Ni 1:10 samples 500 times with LSV at a scan rate of 20 mV/s. Figure 8 shows 500 cycles of Fe-Ni 1:2. We see that after 500 cycles, the onset potential shifts lower (from 1.44 to 1.39 V *vs*. RHE) before overlapping the cycle 1 curve and reaching a similar activity of 22.7 mA/cm^2. This material cycles very well, only losing 3% of its initial activity after 500 cycles.

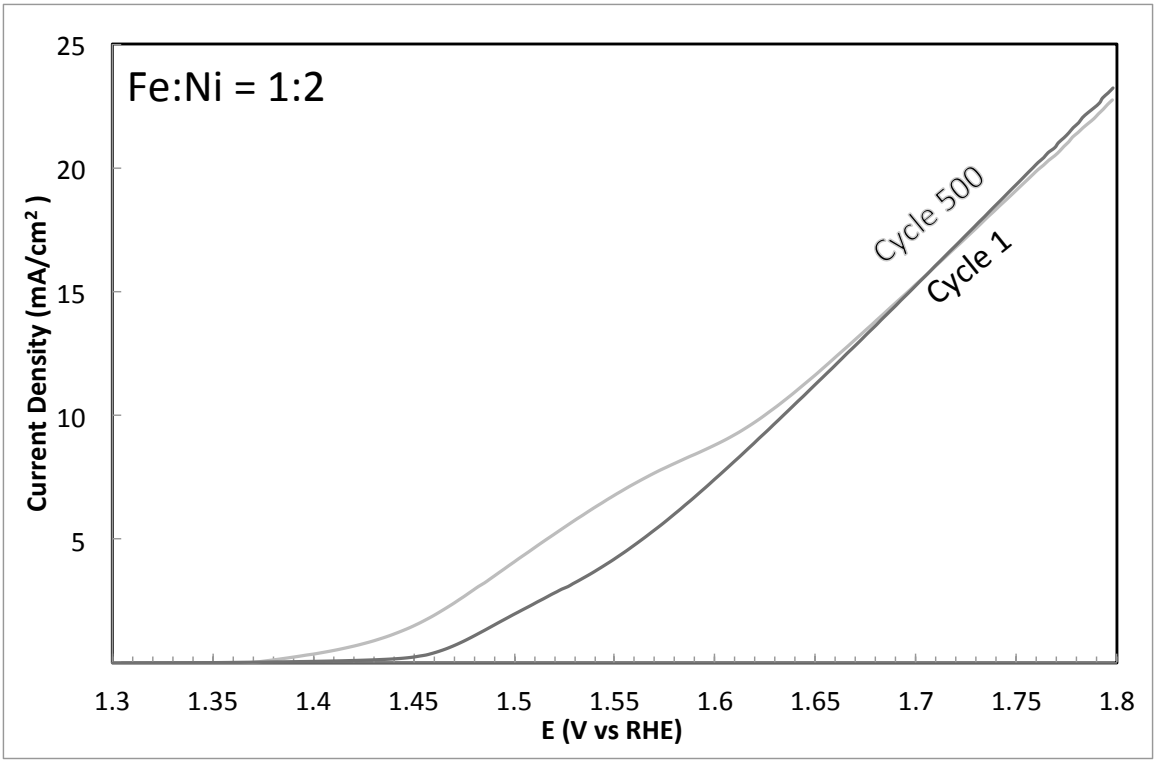

Figure 8: Linear sweep voltammetry (LSV) of Fe-Ni 1:2 for the 1st and 500th cycle.

Such similar activities after 500 cycles indicate that Fe-Ni 1:2 is a very stable material. The onset potential shift could correspond to a transformation of α-$Ni(OH)_2$ to β-$Ni(OH)_2$ [7, 32, 61-66]. It is posited that as the Fe-Ni material ages in an electrolyte, more Fe is incorporated into the inner structure. This causes the onset potential shift as well as an increase in activity after cycling. When we have a closer look at the scans between 1 and 500 cycles (Figure 9), we observe that the activity increases with each cycle for the first 100 cycles. Afterwards, the activity decreases consistently until the

500th cycle. The activity increase is likely due to the α to β-$Ni(OH)_2$ transformation, incorporation of Fe, or the general activation of the catalyst. The subsequent decrease is most likely due to the degradation of CFP support or deactivation of the catalyst [61]. As the material is cycled, bubbles form on the electrode surface, disrupting access, and may lead to decreased activity over time.

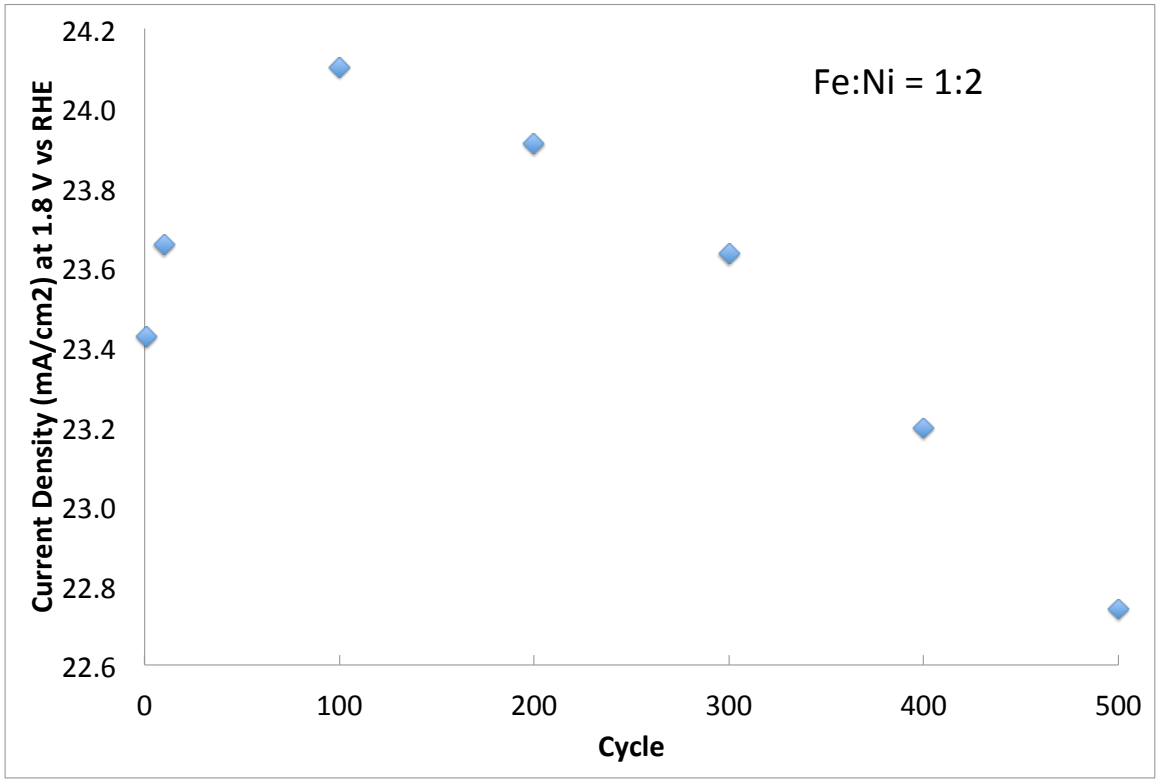

Figure 9: The increase and subsequent decrease of OER activity over 500 cycles at 20 mV/s for Fe-Ni 1:2, taken at 1.8 V *vs*. RHE.

When we focus on the onset potential range of Fe-Ni 1:2 throughout 500 cycles (Figure 10), we notice that the onset potential continuously shifts to lower values. The onset potential shift is likely due to Fe incorporation during cycling [61] or the α-$Ni(OH)_2$ to β-$Ni(OH)_2$ transformation as discussed previously.

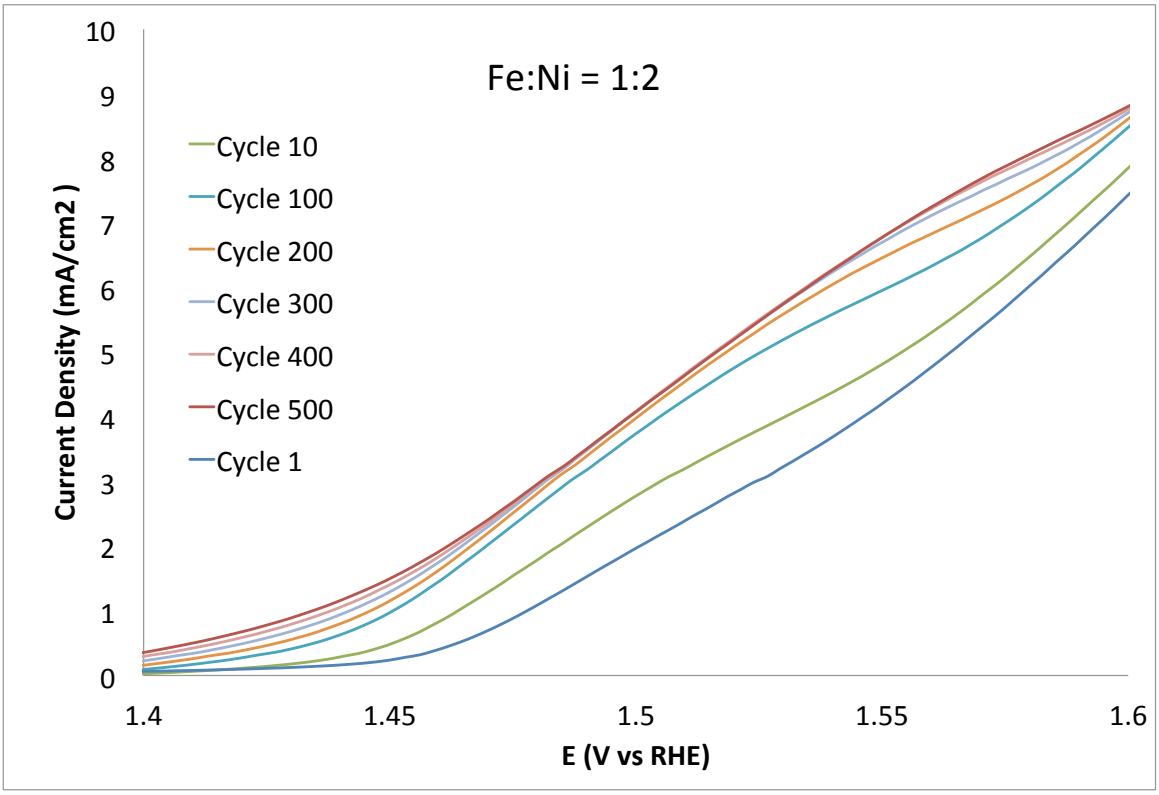

Figure 10: Close-up of the OER onset potential region for Fe-Ni 1:2 during LSV cycle tests.

Overall, Fe-Ni 1:2 performs well. Its onset potential improves with cycling, and the activity only falls slightly over 500 cycles.

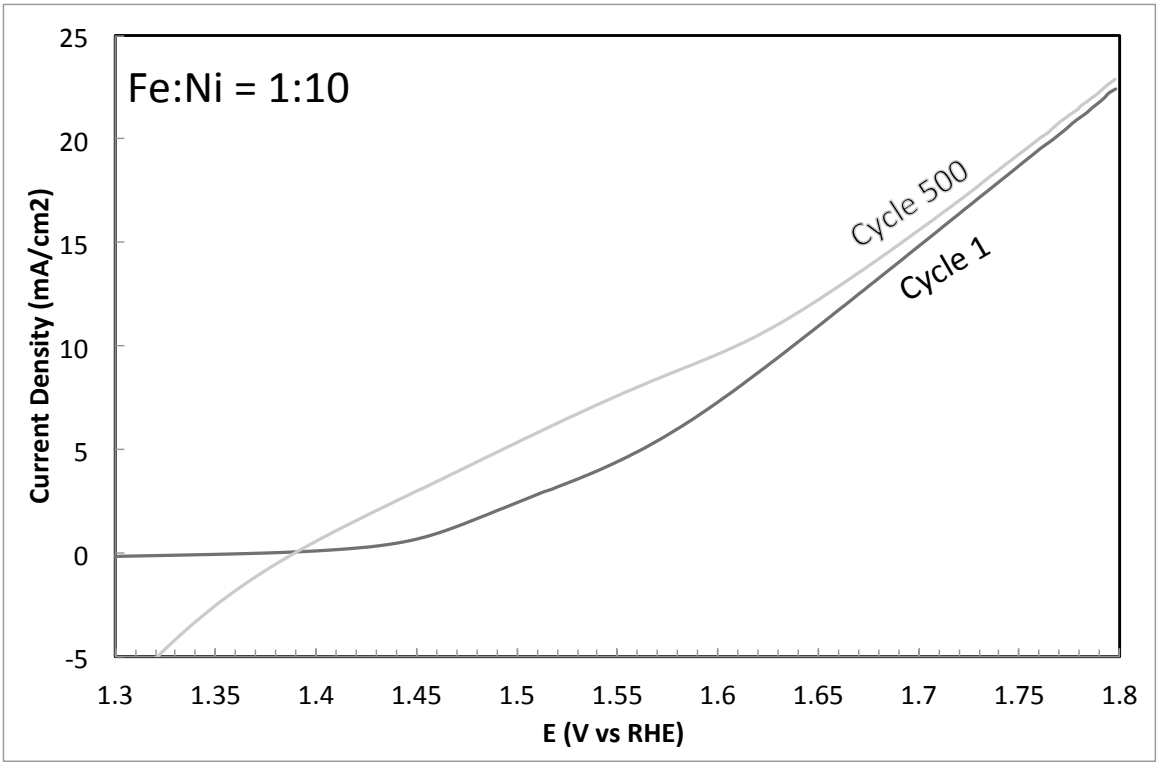

Figure 11: LSV of Fe-Ni 1:10 after 500 cycles.

When we examine Fe-Ni 1:10 in Figure 11, once again we can see that the final activities remain very similar after 500 cycles. In this case they actually increase by 2.2% from 22.5 mA/cm^2 to 22.9 mA/cm^2. The potential shift is very apparent in this sample. In fact, on the 500th cycle, there is no double-layer charging current "baseline" region between 1.3 and 1.4 V *vs*. RHE as seen during the 1st cycle. Instead, the current is negative and increases to positive values with potential.

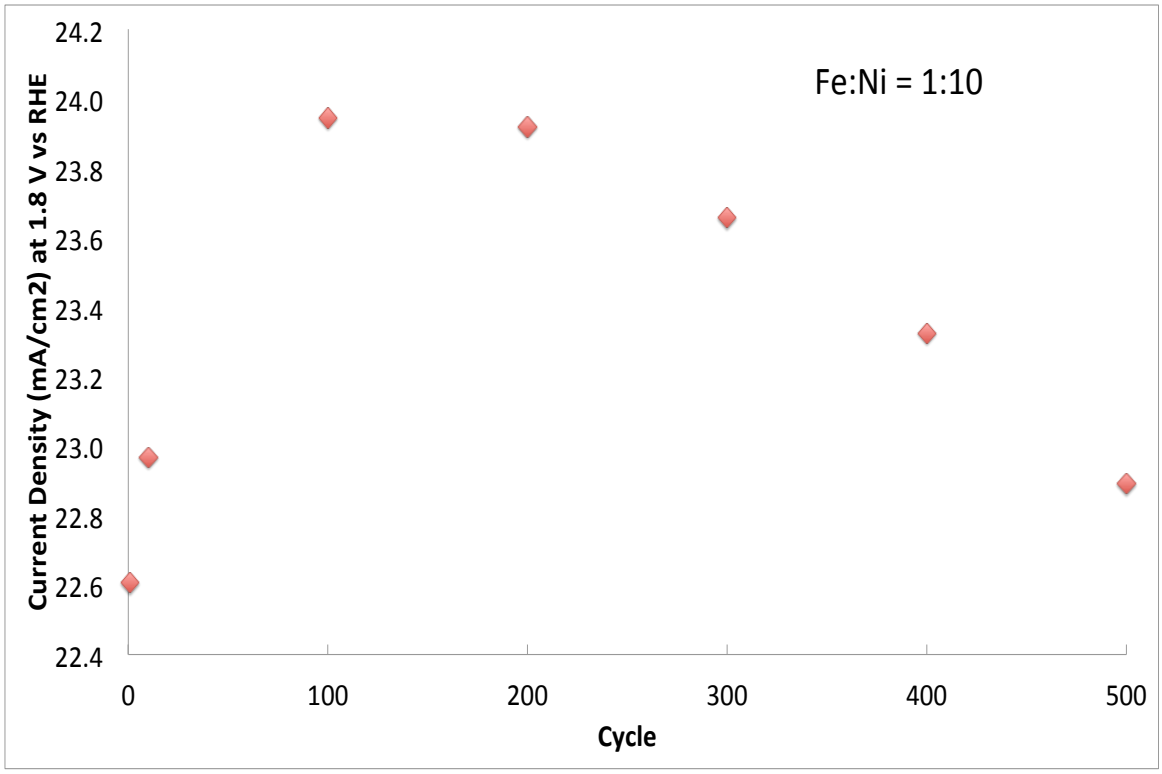

Figure 12: The increase and subsequent decrease of OER activity over 500 cycles during LSV cycling for Fe-Ni 1:10.

When looking at activities over 500 cycles for Fe-Ni 1:10 (Figure 12), we see the same trends as with Fe-Ni 1:2. The activities increase for the first 100 cycles, stay more or less constant from cycles 100 to 200, and decrease for the remaining cycles. Figure 13 shows that the reduction current occurring between 1.3 and ~1.39 V increases as the

cycle number increases. Furthermore, the onset potential for the OER appears to increase from the 1st to the 200th cycle.

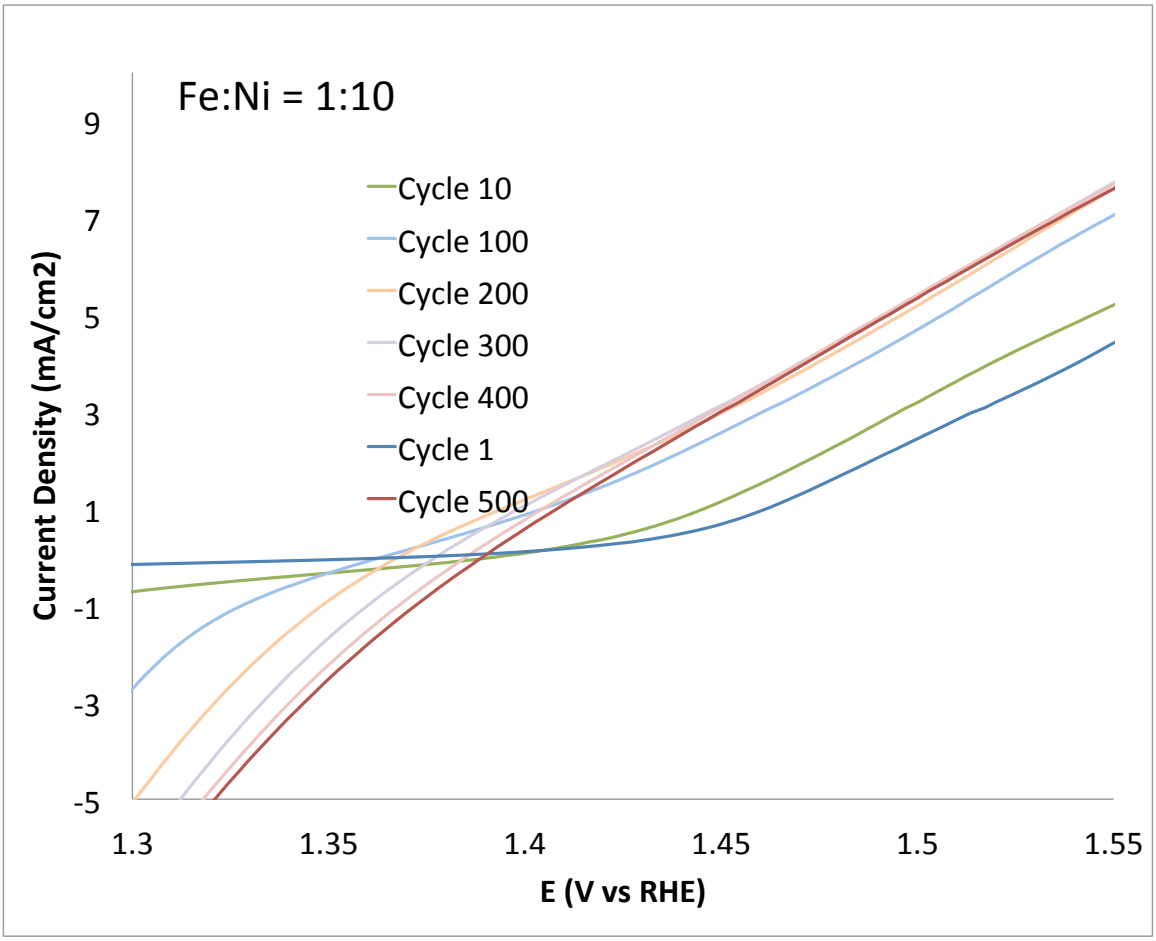

Figure 13: Close-up of the onset potential region for Fe-Ni 1:2 LSV cycle tests.

The increasing-then-decreasing activity trend with cycle number are the same in both samples. Oxygen bubbles may play a role in the decreasing activity trend: in the

first several cycles, OER produces a few small oxygen bubbles on the electrode surface. As the cycle number increases, the OER positive current increases due to activation of the catalyst, and more oxygen is formed. The oxygen bubbles could be interfering with the OER process and cause the degradation. The baseline loss is exclusive to Fe-Ni 1:10 and we must investigate why. One explanation has to do with the nature of the LSV cycling: the linear sweep stops at 1.8 V, and the subsequent cycle begins at 1.3 V, with no reverse scan. The Ni^{3+} generated at highly oxidizing potentials in the linear sweep will be reduced at the beginning of the subsequent cycle, giving rise to a negative current.

Fe-Ni 1:10 is unique in its morphology; this presumably is related to the extreme composition, high Ni content, and low Fe content. The morphology and composition could amplify the CFP degradation, Ni^{3+} reduction, or any other reasons for the trend.

Chapter 4: Conclusions and Future Work

This work examines OER catalysts, composed of Fe-Ni LDHs on CFP, for water electrolysis in alkaline medium. The CFP has shown to be a stable, scalable, support material. The different compositions had very similar morphology, but Fe-Ni 1:10 being slightly less uniform than others. Onset potentials decreased as the Fe:Ni ratio increased, and the activity increased as the Fe:Ni ratio increased. Based on these two criteria, we concluded that the Fe-Ni 1:2 and Fe-Ni 1:10 performed the best, and therefore, they were chosen for further cycle tests.

When the Fe-Ni 1:2 and Fe-Ni 1:10 samples were cycled 500 times, the activity increased for the first 100 cycles and then decreased, most likely due to catalyst activation followed by subsequent degradation. For Fe-Ni 1:10, the lack of 0 mA current baseline region requires further study but may be due to the reduction of Ni^{3+}, formed during the previous cycle, to Ni^{2+}. The Fe-Ni 1:10 onset potential was only slightly less than the Fe-Ni 1:2 but its activity was lower and its cyclic performance was worse. As a result, Fe-Ni 1:2 is the best material overall.

Future work should be aimed at how these electrodes would function in a device, either for electrolysis or in metal-air batteries, with a divided cell with separate OER and ORR catalysts. Future work should also focus on finding the cause of the baseline

degradation. If it is related to the CFP, work should include growing Fe-Ni LDH material on different substrates as others have done [16].

We have successfully grown Fe-Ni material with the same morphology as on Ni-foam, as seen in Figure 14. Using the same initial amounts of $FeCl_2 \cdot 4H_2O$ and $Ni(NO_3)_2 \cdot 6H_2O$ as on CFP, the loading was approximately ten times more, 4.3 mg/cm^2 as opposed to 0.4 mg/cm^2. No electrochemical tests have been performed.

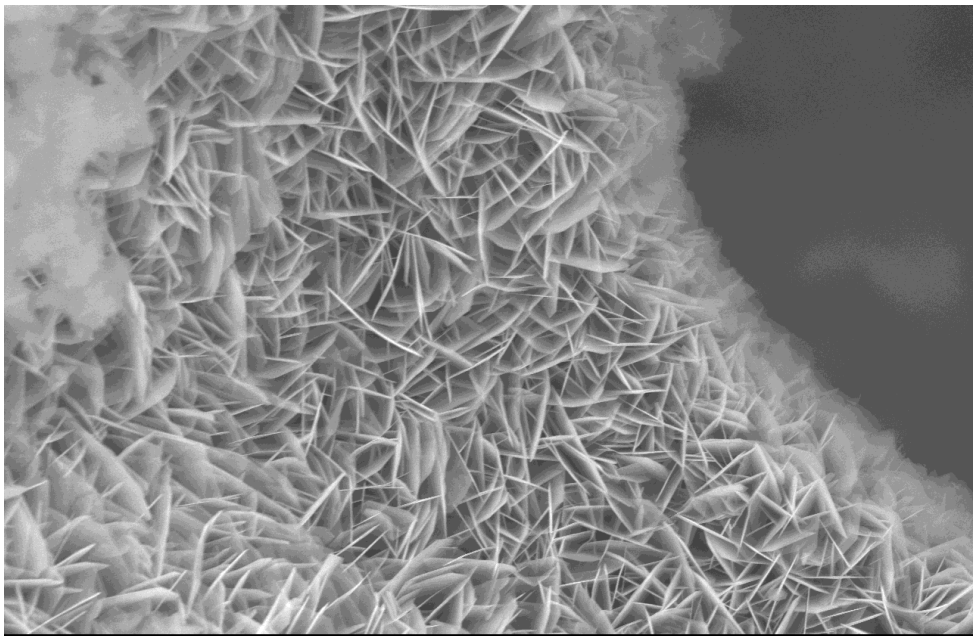

Figure 14: Fe-Ni 1:2 coated on Ni-foam, showing the same morphology as grown on CFP.

References

[1] US Energy Information Administration. "International Energy Outlook (IEO) 2013," [online] available: http://www.eia.gov/forecasts/ieo/world.cfm accessed 25 March 2014.

[2] T.R Cook, DK Dogutan, SY Reece, Y Surendranath, TS Teets and DG Nocera. "Solar Energy Supply and Storage for the Legacy and Nonlegacy Worlds." *Chemical Reviews*. 2010, 110, 6474.

[3] EL Miller, RE Rocheleau, "Electrochemical Behaviour of Reactively Sputtered Iron-Doped Nickel Oxide." *Journal of the Electrochemical Society*. 1997, 144, 1995.

[4] RDL Smith, MS Prévot, RD Fagan, ZP Zhang, PA Sedach, MKJ Siu, S Trudel, CP Berlinguette. "Photochemical Route for Accessing Amorphous Metal Oxide Materials for Water Oxidation Catalysis." *Science*. 2013, 340, 60.

[5] H Lin, Y Zhang, G Wang and JB Li. "Cobalt-based layered double hydroxides as an oxygen evolving electrocatalysts in neutral electrolyte." *Frontiers of Materials Science*. 2012, 6, 142-148.

[6] X Tang, L Xiao, C Yang, J Ly and L Zhuang, "Noble fabrication of Ni-Mo cathode for alkaline water electrolysis and alkaline polymer electrolyte water electrolysis." *International Journal of Hydrogen Energy*. 2014, 39, 3055-3060.

[7] M Louie and A Bell, "An investigation of thin-film Ni-Fe oxide catalysts for the electrochemical evolution of oxygen." *Journal of the American Chemical Society*. 2013, 135, 12329-12337.

[8] J Landon, E Demeter, N Inoglu, C Keturakis, I Wachs, R Vasic, A Frenkel, and J Kitchin, "Spectroscopic characterization of Mixed Fe-Ni oxide Electrocatalysts for the oxygen evolution reaction in alkaline electrolytes." *ACS Catalysis*. 2012, 2, 1793-1801.

[9] P Refait and J Genin, "Mechanisms of oxidation of Ni(II)-Fe(II) hydroxides in chloride-containing aqueous media: role of the pyroaurite-type Ni-Fe hydroxychlorides." *Clay Minerals*. 1997, 32, 597-613.

[10] YF Li and A Selloni, "Mechanism and activity of water oxidation on selected surfaces of pure and Fe-Doped NiOx." *ACS Catalysis*. 2014, 4, 1148-1153.

[11] Y Zhang, B Cui, C Zhao, H Lin and J Li. "Co-Ni layered double hydroxides for water oxidation in neutral electrolyte." *Physical Chemistry Chemical Physics*. 2013, 15, 7363.

[12] R Doyle and M Lyons, "An electrochemical impedance study of the oxygen evolution reaction at hydrous iron oxide in base." *Physical Chemistry Chemical Physics*, 2013, 15, 5224.

[13] L Trotochaud, S Boettcher, "Precise oxygen evolution catalysts: Status and opportunities." *Scripta Materialia*. 2013, 74, 25-32.

[14] SW Lee, C Carlton, M Risch, Y Surendranath, S Chen, S Furutsuki, A Yamada, D Nocera and Y Shao-Horn, "The Nature of Lithium Battery Materials under Oxygen Evolution Reaction Conditions." *Journal of the American Chemical Society*. 2012, 134, 16959-16962.

[15] L Trotochaud, JK Ranney, KN Williams and SW Boettcher. "Solution-Cast Metal Oxide Thin Film Electrocatalysts for Oxygen Evolution." *Journal of the American Chemical Society*. 2012, 134, 17253-17261.

[16] FJ Perez-Alonso, C Adan, S Rojas, MA Pena, JLG Fierro. "Ni/Fe electrodes prepared by electrodeposition method over different substrates for oxygen evolution reaction in alkaline medium." *International Journal of Hydrogen Energy*. 2014, 39, 5204-5212.

[17] M Gong, Y Li, H Wang, Y Liang, J Wu, J Zhou, J Wang, T Regier, F Wei and J Dai. "A Ni-Fe Layered double Hydroxide-Carbon Nanotube Complex for Water Oxidation." Eprint arXiv:1303.3308. 2013.

[18] M Gong, Y Li, H Wang, Y Liang, J Wu, J Zhou, J Wang, T Regier, F Wei and J Dai. "An Advanced Ni-Fe Layered Double Hydroxide Electrocatalyst for Water Oxidation." *Journal of the American Chemical* Society. 2013, 135, 8452-8455.

[19] R Ramachandran and R Menon, "An overview of industrial uses of hydrogen." *International Journal of Hydrogen Energy*. 1998, 23, 7, 593-598.

[20] D Evans, R Slade, "Structural aspects of layered double hydroxides." 2006, Struct Bond. DOI 10.1007/430_005.

[21] X Liang, Y Zang, Y Xu, X Tan, W Hou, L Wang, Y Sun, "Sorption of metal cations on layered double hydroxides." *Colloids and Surfaces A: Physiochemical and engineering aspects*. 2013, 433, 122-131.

[22] HJ Neef, "International overview of hydrogen and fuel cell research." *Energy*. 2009, 34, 327-333.

[23] H Dau, C Limberg, T Reier, M Risch, S Roggan,
P Strasser, "The Mechanism of Water Oxidation: From Electrolysis via Homogeneous to Biological Catalysis." *ChemCatChem*, 2010, 2, 724.

[24] J Sunarso, AM Glushenkov, A Torriero, P Howlett, Y Chen, D MacFarlane and M Forsyth, "Bi-Functional Water/Oxygen Electrocatalyst Based on PdO-RuO2 Composites." *Journal of the Electrochemical Society*. 2013, 160, 74-79.

[25] K Tomohito, S Shingo and U Yoshiaki. "Mg-Al layered double hydroxide intercalated with ethylene diaminetetraacetate anion: Synthesis and application to the uptake of heavy metal ions from an aqueous solution." *Separation and Purification Technology*. 2005, 47, 20-26.

[26] R Ma, Z Liu, K Takada, N Iyi, Y Bando and T Sasaki, "Synthesis and exfoliation of Co2+-Fe3+ layered double hydroxides: An innovative topochemical approach." *Journal of the American Chemical Society*. 2007, 129, 5257-5263.

[27] S Bhattacharjee, TJ Dines and JA Anderson. "Comparison of Co with Mn and Fe in LDH-hosted Sulfonato-Salen Catalysts for Olegin Epoxidation." *The Journal of Physical Chemistry C*. 2008, 112, 14124.

[28] JO Bockris, T Qtagawa. "The Electrocatalysis of Oxygen Evolution on Perovskites." *Journal of the Electrochemical Society*. 1984, 131, 290.

[29] J Chen, DH Bradhurst, SX Dou, HK Liu, "Nickel hydroxide as an active material for the positive electrode in rechargeable alkaline batteries." *Journal of the Electrochemical Society*. 1999, 146, 3606.

[30] DA Corrigan, "The catalysis of the oxygen evolution reaction by iron impurities in thin film nickel oxide electrodes." *Journal of the Electrochemical Society*. 1987, 134, 377.

[31] DA Corrigan, SL Knight, "Electrochemical and spectroscopic evidence on the participation of quadrivalent nickel in the nickel hydroxide redox reaction." *Journal of the Electrochemical Society*. 1989, 136, 613.

[32] DA Corrigan, RM Bendert, "Effect of coprecipitated metal ions on the electrochemistry of nickel hydroxide thin films: cyclic voltammetry in 1M KOH." *Journal of the Electrochemical Society*. 1989, 136, 723.

[33] PWT Lu, S Srinivasan, "Electrochemical-ellipsometric studies of oxide film formed on nickel during oxygen evolution." *Journal of the Electrochemical Society*. 1978, 125, 1416.

[34] Department of Solid State Chemistry, Institute of Chemical Technology, Prague, Technická 5, 166 28 Prague, Czech Republic. [online] available: http://tresen.vscht.cz/min/en/research-team-mineralogy accessed 12 March 2014.

[35] T Xiao, Y Tang, Z Jia, D Li, X Hu, B Li and L Luo. "Self-assembled 3D flower-like Ni^{2+}-Fe^{3+} layered double hydroxides and their calcined products." *Nanotechnology*. 2009, 20, (47), 475603-47610.

[36] H Li, G Zhu, Z Yang, Z Wang and Z-H Liu. "Preparation and capacitance property of MnO_2-pillared Ni^{2+}-Fe^{3+} layered double hydroxides nanocomposite." *Journal of Colloid and Interface Science*. 2010, 345, (2), 228-233.

[37] Y Han, ZH Liu, Z Yang, Z Wang, Z Tang, T Wang, L Fan and K Ooi. "Preparation of Ni^{2+}-Fe^{3+} Layered Double Hydroxide Material with High Crystallinity and Well-Defined Hexagonal Shapes." *Chemistry of Materials*. 2008, 20, 360-363.

[38] F Boukraa, D Saiah, BL Su and N Bettahar. "Nickel-iron layered double hydroxide (LDH): Textural properties upon hydrothermal treatments and application on dye sorption." *Journal of Hazardous Materials*. 2009, 165, 206-217.

[39] Y Li, H Li, M Yang, X He, P Ni, L Kang and ZH Liu. "Topochemical synthesis of Ni^{2+}-Fe^{3+} layered double hydroxides with large size." *Applied Clay* Science. 2011, 52, 51-55.

[40] G Abellan, E Coronado, C Marti-Gastaldo, E Pinilla-Cienfuegos and A Ribera. "Hexagonal nanosheets from the exfoliation of Ni^{2+}-Fe^{3+} LDHs: a route towards layered multifunctional materials." *Journal of Materials Chemistry*. 2010, 20, 7451-7455.

[41] E Coronado, J Galan-Mascaros, C Marti-Gastaldo, A Ribera, E Palacios, M Castro and R Burriel, "Spontaneous Magnetization in Ni-Al and Ni-Fe Layered Double Hydroxides." *Inorganic Chemistry*. 2008, 47, 9103-9110.

[42] X Xiang, H Hima, H Wang and F Li, "Facile synthesis and catalytic properties of nickel-based mixed-metal oxides with mesopore networks from a novel hybrid composite precursor." *Chemistry of Materials*. 2008, 20, 1173-1182.

[43] PC Pavan, GA Gomes and JB Valim. "Adsorption of sodium dodecyl sulfate on layered double hydroxides." *Microporous and Mesoporous Materials*. 1998, 21, 659-665.

[44] YF Wang and HZ Gao. "Compositional and structural control on anion sorption capability of layered double hydroxides (LDHs)." *Journal of Colloid and Interface Science*. 2006, 301, 19-26.

[45] DL Bish. "Anion-exchange in takovite: application to other hydroxide minerals." *Bull. Mineral*. 1980, 103, 170-175.

[46] KH Goh, TT Lim, Z Dong, "Application of layered double hydroxides for removal of oxyanions: A review." *Water Research*. 2008, 42, 1343-1368.

[47] M Darder, M Lopez-Blanco, P Aranda, F Leroux and E Ruiz-Hitzky. "Bio-Nanocomposites Based on Layered Double Hydroxides." *Chemistry of Materials*. 2005, 17, 1969-1977.

[48] C Forano, S Vial and C Mousty. "Nanohybrid Enzymes – Layered Double Hydroxides: Potential Applications." *Current Nanoscience*. 2006, 2, 283-294.

[49] D Francova, N Tanchoux, C Gerardin, P Trens, F Prinetto, G Ghiotti, D Tichit and B Coq. "Hydrogenation of 2-butyne-1,4-diol on supported Pd catalysts obtained from LDH precursors." *Microporous and Mesoporous Materials*. 2007, 99, 118-125.

[50] Y Liu, K Murata, T Hanaoka, M Inaba and K Sakanish. "Synthesis of new peroxo-polyoxometalates intercalated layered double hydroxides for propene epoxidation by molecular oxygen in methanol." *Journal of Catalysis*. 2007, 248, (2), 277-287.

[51] B Sels, D De Vos, M Buntinx, F Pierard, A Mesmaiker and P Jacobs. "Layered double hydroxides exchanged with tungstate as biomimetic catalysts for mild oxidative bromination." *Nature*. 1999, 400, 855-857.

[52] Z Wang, F Liu and C Lu, "Mg-Al-carbonate layered double hydroxides as a novel catalyst of luminol chemiluminescence." *Chemical Communications*. 2011, 47, 5479-5481.

[53] J Zhao, Z Lu, M Shao, D Yan, M Wei, D Evans and X Duan. "Flexible hierarchical nanocomposites based on MnO2 nanowires/CoAl hydrotalcite/carbon fibers for high-performance supercapacitors." *RSC Advances*. 2013, 3, 1045.

[54] J Zhao, J Chen, S Xu, M Shao, D Yan, M Wei, D Evans and X Duan. "CoMn-layered double hydroxide nanowalls supported on carbon fibers for high-performance flexible energy storage devices." *Journal of Materials Chemistry A*. 2013, 1, 8836-8843.

[55] G Zhang and XW Lou. "General Solution Growth of Mesoporous $NiCo_2O_4$ Nanosheets on Various Conductive Substrates as High-Performance Electrodes for Supercapacitors." *Advanced Materials*. 2013, 25, 976-979.

[56] L Yang, S Cheng, Y Ding, X Zhy, ZL Wang and M Liu. "Hierarchical Network Architectures of Carbon Fiber Paper Supported Cobalt Oxide Nanonet for High-Capacity Pseudocapacitors." *Nano Letters*. 2012, 12 (1), 321-325.

[57] B Yang and Z Yang. "Structure and improved electrochemical performance of a nanostructured layered double hydroxide-carbon nanotube composite as a novel anode material for Ni-Zn secondary batteries." *RSC Advances*. 2013, 3, 12589-12592.

[58] X Wang, S Zhou, W Xing, B Yu, X Feng, L Song and Y Hu, "Self-assembly of Ni-Fe layered double hydroxide/grapheme hybrids for reducing fire hazard in epoxy composites." *Journal of Materials Chemistry A*. 2013, 1, 4383-4390.

[59] C Zu, YS Su, Y Fu and A Manthiram, "Improved Lithium-sulfur cells with a treated carbon paper interlayer." *Physical Chemistry Chemical Physics*. 2013, 15, 2291-2297.

[60] X Zhang, Z Shen, "Carbon fiber paper for fuel cell electrode." *Fuel*. 2002, 81, 17, 2199-2201.

[61] L Trotochaud, S Young, J Ranney, S Boettcher. "Nickel-Iron Oxyhydroxide Oxygen-Evolution Electrocatalysts: The Role of Intentional and Incidental Iron Incorporation." *Journal of the American Chemical Society*. 2014.

[62] AJ Bard, LR Faulkner, "Electrochemical Methods." John Wiley and Sons, Inc, 2001.

[63] MC Bernard, P Bernard, M Keddam, S Senyarich, H Takenouti, "Characterization of new Nickel hydroxides during the transformation of A $Ni(OH)_2$ to B $Ni(OH)_2$ by ageing." *Electrochimica Acta*. 1996, 41, 91.

[64] MS Kim, KB Kim, "A study on the phase transformation of electrochemically precipitated nickel hydroxides using an electrochemical quartz crystal microbalance." *Journal of the Electrochemical Society*. 1998, 145, 507.

[65] M Wehrens-Dijksma, PHL Notten, "Electrochemical quartz microbalance characterization of $Ni(OH)_2$-based thin film electrodes." *Electrochimica Acta*. 2006, 51, 3609.

[66] J Nan, Y Yang, Z Lin, “In situ photoelectrochemistry and Raman spectroscopic characterization on the surface oxide film of nickel electrode in 30 wt. % KOH solution.” *Electrochimica Acta*. 2006, 51, 4873.